
ZERO-SHOT SEGMENTATION OF EYE FEATURES USING THE SEGMENT ANYTHING MODEL (SAM)

A PREPRINT

Virmarie Maquiling

Human-Centered Technologies for Learning
Technical University of Munich
virmarie.maquiling@tum.de

Sean Anthony Byrne

MoMiLab
IMT School for Advanced Studies Lucca
sean.byrne@imtlucca.it

Diederick C. Niehorster

Lund University Humanities Lab &
Dept. of Psychology
Lund University
diederick_c.niehorster@humlab.lu.se

Marcus Nyström

Lund University Humanities Lab
Lund University
marcus.nystrom@humlab.lu.se

Enkelejda Kasneci

Human-Centered Technologies for Learning
Technical University of Munich
enkelejda.kasneci@tum.de

November 15, 2023

ABSTRACT

The advent of foundation models signals a new era in artificial intelligence. The Segment Anything Model (SAM) is the first foundation model for image segmentation. In this study, we evaluate SAM's ability to segment features from eye images recorded in virtual reality setups. The increasing requirement for annotated eye-image datasets presents a significant opportunity for SAM to redefine the landscape of data annotation in gaze estimation. Our investigation centers on SAM's zero-shot learning abilities and the effectiveness of prompts like bounding boxes or point clicks. Our results are consistent with studies in other domains, demonstrating that SAM's segmentation effectiveness can be on-par with specialized models depending on the feature, with prompts improving its performance, evidenced by an IoU of 93.34% for pupil segmentation in one dataset. Foundation models like SAM could revolutionize gaze estimation by enabling quick and easy image segmentation, reducing reliance on specialized models and extensive manual annotation.

Keywords Eye-tracking, Segmentation, Segment Anything Model, Zero-shot learning, Foundational models, Prompt Engineering

1 Introduction

Foundation models and Generative AI are already being celebrated as the groundbreaking developments of the decade in the realm of artificial intelligence. They mark a significant paradigm change in the way users interact, develop, and deploy deep learning models Bommasani et al. (2022). Compared to traditional deep learning models, foundation models have scalable attributes, such as the vast number of trainable parameters and the extensive amounts of data they are trained on. Due to these scaling attributes foundational models demonstrate a remarkable ability to adjust to downstream tasks and exhibit proficiency on data distributions previously unseen during their training phase Kirillov et al. (2023); Bommasani et al. (2022). From a non-technical standpoint, these models have made it easier to utilize

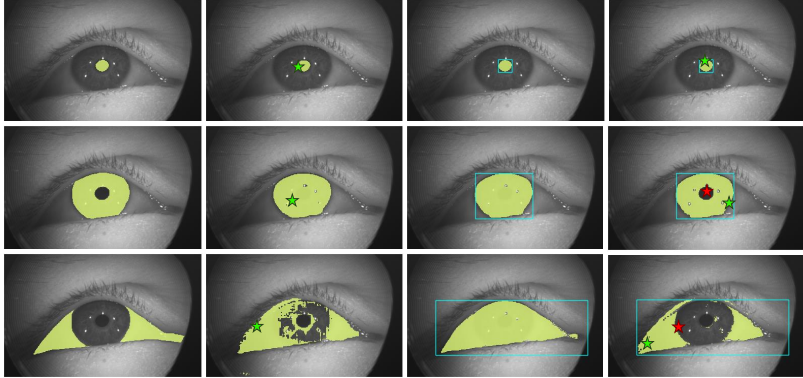


Figure 1: Visualization of SAM’s segmentation performance according to strategy. On the leftmost column are the ground truth masks for key eye features: pupil, iris, and sclera. The remaining columns show representative prompt strategies used in the experiment overlaid with the resulting masks generated by SAM. Green and red stars represent foreground and background point prompts. The light blue rectangle represents a bounding box prompt.

tools powered by artificial intelligence, managing complex tasks that previously required specialized supervised learning models, and often custom datasets collected specifically for the problem at hand Bommasani et al. (2022); Zhou et al. (2023b). In contrast, foundation models simplify the deployment process through their innate zero-shot learning capabilities—where the model makes accurate predictions on tasks without having seen any examples during training Romera-Paredes and Torr (2015). This potential can be further improved with straightforward prompts. These prompts can be as easy to create as a single mouse click or circling a significant feature within an image, thereby diminishing the complexity and time needed to apply deep learning models on a large scale Mazurowski et al. (2023).

In this study, we harness the power of the Segment Anything Model (SAM) Kirillov et al. (2023), the first foundation model developed for image segmentation, and which has demonstrated remarkable abilities within a variety of different domains, including both natural and specialized forms of imagery, such as medical imaging Ma et al. (2023), and remote sensing Archit et al. (2023). We apply SAM in the context of gaze estimation, where we task the model to segment eye regions in near-eye images obtained from a virtual reality (VR) setting. We investigate a variety of prompting strategies to bolster SAM’s performance and closely examine its effectiveness in identifying three specific ocular regions: the pupil, iris, and sclera. Annotating eye regions, a well-known task within video-based eye-tracking, is both subjective and costly in terms of time. These segmented features are essential not only for precise gaze estimation but also as training data for specialized deep learning models that require numerous annotated examples in order to make accurate predictions.

In addition to their ease of deployment, foundation models like SAM hold promise in overcoming the domain generalization issue—a notable obstacle across machine learning, where models typically falter when applied to data different from their training set Zhou et al. (2022). This challenge is particularly evident in gaze estimation, where it has been noted that many supervised learning models, such as convolutional neural networks, often fail to generalize their understanding of eye components, resulting in subpar performance on data not encountered during their training due to differences in recording setup such as lighting, camera angle, and any physiological differences across participants Kothari et al. (2022); Byrne et al. (2023a); Kim et al. (2019). The development of extensive datasets recorded across multiple devices Fuhl et al. (2021); Kothari et al. (2022) and the generation of synthetic data Kim et al. (2019); Nair et al. (2020); Maquiling et al. (2023); Byrne et al. (2023a) have been suggested to bypass the domain generalization problem in gaze estimation. Yet, these approaches haven’t completely resolved the issue and also introduce significant entry barriers, including the need for substantial computational power and specialized expertise in computer vision. However, foundation models have showcased exceptional generalization abilities, both in zero-shot and few-shot scenarios, adeptly adapting to unseen tasks and data distributions Brown et al. (2020); Bommasani et al. (2022).

Our investigation is threefold. First, we provide a literature review on foundation models, zero-shot learning, and eye image segmentation to give the reader a clear understanding of the problem and potential of foundation models in this domain. Second, we explain what it means for a model like SAM to be “promptable” and introduce a set of prompting strategies designed to explore SAM’s capabilities for eye image segmentation. Third, using these tailor-made prompting strategies, we evaluate SAM’s performance on two public eye image segmentation datasets, providing quantitative and qualitative analysis with the aim of illuminating the potential and limitations of applying SAM to the domain of

eye tracking. Our results reveal that SAM, in a zero-shot learning context, can produce annotations that rival manual annotations derived from experts and annotations from traditional supervised learning models in segmenting the pupil, even with minimal manual guidance. Nevertheless, the model exhibits certain limitations in the accurate annotation of the sclera and, to a lesser degree, the iris. We have made all code available to users at the following repository [HIDDEN FOR REVIEW] for both benchmarking and labeling their own datasets.

2 RELATED WORK

2.1 An Introduction to Foundation models

Foundation models are a relatively new concept in deep learning, and as such, there is not an extensive amount of literature available on them yet. Although these models first gained prominence in the realm of Natural Language Processing (NLP), they have recently made significant strides in the field of computer vision. Foundation models are large-scale machine-learning models trained on massive amounts of data that can be adapted for a wide range of downstream tasks. These models mark a departure from conventional deep learning approaches due to their scale, boasting not only an unprecedented number of parameters (up to hundreds of billions) but also being pre-trained on extensive datasets. This enables them to adapt to a variety of tasks through fine-tuning and to exhibit emergent behaviors, such as strong performance on previously unseen data distributions Bommasani et al. (2022). Leading the way are models like BERT Devlin et al. (2018), Generative Pre-Trained Transformers (GPTs) Brown et al. (2020), and CLIP Radford et al. (2021), all of which leverage large-scale data for training. ChatGPT, fine-tuned from the GPT-3 model with its 175 billion parameters, excels in various tasks through natural language prompts and has significantly influenced AI over the last year Zhou et al. (2023b). Already, there is a growing trend toward the creation of specialized foundation models, such as MedSAM for medical imaging Ma et al. (2023), and even more domain-specific, RETFound, a model designed specifically for the analysis of retinal images Zhou et al. (2023a). For a comprehensive review of foundation models see Bommasani et al. (2022).

2.2 The Segment Anything Model

The Segment Anything model (SAM) Kirillov et al. (2023) is a state-of-the-art vision transformer trained on the SA-1B dataset, a collection of diverse images (11 million) accompanied by high-quality segmentation masks (1.1 billion) created specifically for SAM’s training, making it the largest publicly available image segmentation dataset to date. The dataset was generated in three stages. In the first stage, a set of images was labeled by a team of professional annotators by clicking on foreground and background points and refining masks generated by an early version of SAM that was trained on common public segmentation datasets. In the second stage, SAM automatically generated masks of a subset of the dataset, while the annotators focused on annotating the rest of the objects to increase mask diversity. In the last stage, the remaining masks were automatically generated by SAM by prompting the model with a 32×32 grid of foreground points Kirillov et al. (2023).

In order to enable zero-shot generalization in image segmentation tasks, a novel promptable segmentation task was introduced Kirillov et al. (2023), in which, given an image and any prompt, the goal is to return a valid segmentation mask. In this context, a “prompt” specifies which object needs to be segmented by the model, e.g. by providing spatial information. This can be manually given by a user or generated by a different model (e.g. using an object detection model).

To support this novel promptable task, the model, as depicted in Fig. 2, consists of three main components (for a more detailed description, refer to the original paper Kirillov et al. (2023)):

- **Image encoder:** This uses a Vision Transformer Dosovitskiy et al. (2010), pre-trained using Masked Autoencoders (MAE) He et al. (2022), as its backbone and can be run once per image before prompting the model. The image encoder uses an input resolution of 1024×1024 by resizing and padding the input image. It then outputs a $16 \times$ downsampled image embedding of size 64×64 .
- **Prompt encoder:** This encoder accepts sparse (points, boxes, text) and dense (masks) prompts and encodes them as positional embeddings (points and boxes), by CLIP Radford et al. (2021) (text), or through convolutions (masks). Point prompts are given as pixel coordinates in the image, accompanied by point labels indicating whether each corresponding point is in the foreground or the background. Bounding box prompts consist of a pair of pixel coordinates indicating the top-left corner and the bottom-right corner of the box. For information regarding other prompt modes, refer to the original paper Kirillov et al. (2023).
- **Mask decoder:** This lightweight decoder maps the image and prompt embeddings to an output mask.

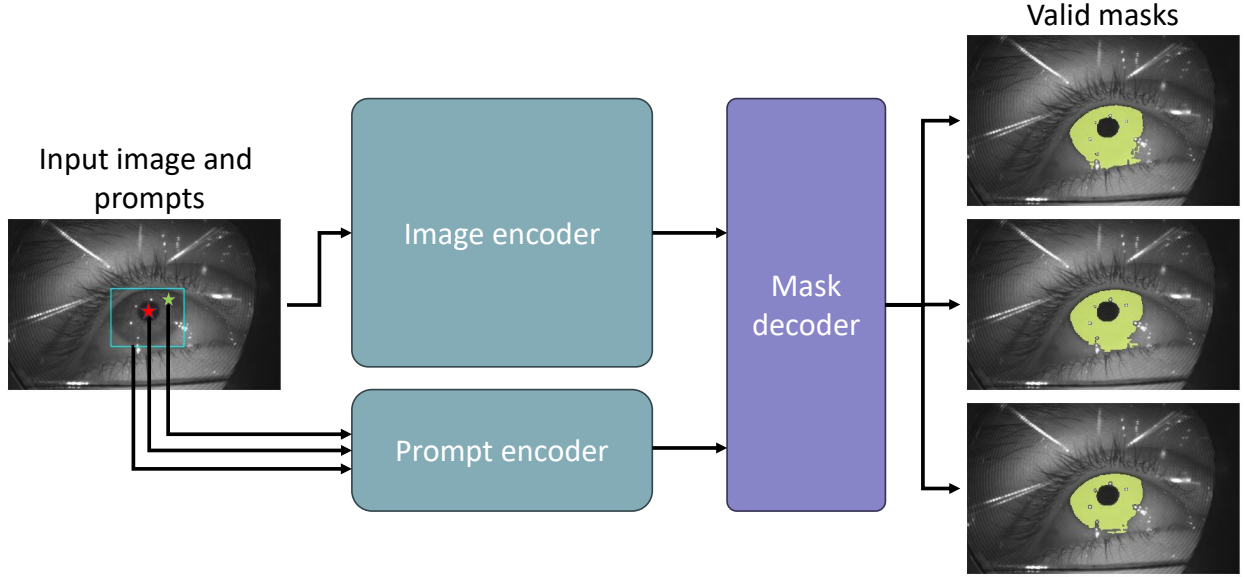


Figure 2: A high-level schematic of the Segment Anything Model (SAM) featuring an image encoder, a prompt encoder, and a lightweight mask encoder. The image is fed to the image encoder, while a set of prompts (in this example, depicted as point- and bounding box prompts drawn on the image) are fed to the prompt encoder. The embeddings generated by the image and prompt encoders are passed to the mask decoder which outputs valid masks with varying confidence scores. Alternatively, it may output a single mask averaged over all valid masks.

SAM supports two modes: an automatic “everything” mode, in which the user simply inputs an image to SAM, which then returns all predicted masks found within the image, and a manual mode which expects the user to input an image and a combination of manual prompts to indicate the location of the object to be segmented, e.g. by simply clicking on the image or drawing a bounding box around the region of interest.

Three pre-trained models of varying network sizes are available in SAM’s GitHub repository¹. From smallest to largest, they are named ViT Base (ViT-B), Vit Large (ViT-L), and Vit Huge (ViT-H). The authors report substantial improvement of ViT-H over ViT-B, while showing only marginal improvement over ViT-L. However, due to its increased complexity, inference time is also multiplied Kirillov et al. (2023). Nevertheless, previous work reported that ViT-H did not show a significant advantage over ViT-B, with ViT-B even surpassing larger variants in some segmentation tasks Huang et al. (2023); Mattjie et al. (2023).

2.3 Applications of the Segment Anything Model

The application of the Segment Anything Model (SAM) has already been broad, extending to various domains and specialized tasks, with adaptations that have seen it being used in video tracking Yang et al. (2023) and three-dimensional environments Shen et al. (2023). However, this literature review section will focus exclusively on the downstream performance of the original SAM architecture. To our knowledge, there exists only a singular study where SAM has been integrated with eye-tracking data: GazeSAM Wang et al. (2023a). This model enhances the automation of medical image segmentation by capturing the eye movements of radiologists and using this gaze data to prompt SAM for interactive segmentation tasks. SAM has been notably utilized in medical imaging in many studies. One study demonstrates SAM’s versatility across 19 different medical imaging datasets by employing interactive point and box prompts in a zero-shot segmentation task. The outcomes showed variable Intersection Over Union (IOU) scores depending on the specific dataset and segmentation task, with scores fluctuating from 0.1135 in spine datasets to 0.8650 in MRI images Mazurowski et al. (2023). These findings were largely corroborated in a separate study, which emphasized SAM’s capacity to minimize annotation time in medical image analysis Huang et al. (2023). This study also concluded that SAM benefits from point and box prompts to enhance object detection in medical images, yet much like in the aforementioned work Mazurowski et al. (2023) its performance remains inconsistent across different objects and modalities. Taking this a step further, researchers created MedSAM, a foundational model specifically for medical images Ma et al. (2023). The study leveraged the SAM dataset to pre-train a transformer model, which was

¹<https://github.com/facebookresearch/segment-anything/>

then fine-tuned using over 1 million medical images. The MedSAM model not only surpassed the standard SAM in performance but also matched or exceeded specialized models, like a U-net, which are tailored for particular medical imaging tasks Ma et al. (2023). Outside of medical imaging, SAM has been applied in domains such as graphs Jing et al. (2023), remote sensing Wang et al. (2023b) and microscopy Archit et al. (2023) all with various degrees of success depending on the task.

2.4 Segmentation of eye-images recorded using video-based eye-tracking systems

In the context of image analysis for video-based eye-tracking, segmentation is an essential process that typically involves the detection and segmentation of areas such as the pupil, sclera, iris, and any corneal reflections according to the specific requirements of the task. Pupil center localization is a core part of many gaze estimation methodologies Kim et al. (2019). Additionally, techniques that track both the pupil and corneal reflections (P-CR eye tracking) are widely employed for gaze estimation, representing the leading approach in the video-based eye-tracking sector Dunn et al. (2023). Limbus tracking, which uses the boundary between the iris and sclera, is another technique utilized for gaze and eye movement monitoring Holmqvist et al. (2011).

Historically, the segmentation of eye images from video footage was often done using computer vision techniques, such as ellipse fitting or thresholding methods. These techniques rely on handcrafted algorithms and heuristics to identify features Kothari et al. (2022); Santini et al. (2018). Despite their effectiveness, they can fail in the presence of, for instance, occlusions, changing illumination conditions, or reflections in the eye images Fuhl et al. (2016b). A potential remedy has been the adoption of machine learning and, subsequently, deep learning models, which have considerably enhanced the robustness of gaze estimation algorithms Kothari et al. (2022); Fuhl et al. (2016a, 2022). The issue of data scarcity and the aspiration to tackle domain generalization issues have led to propositions for both large-scale Fuhl et al. (2021); Kothari et al. (2022) and synthetic datasets Byrne et al. (2023b,a); Kim et al. (2019); Maquiling et al. (2023); Nair et al. (2020). These are intended as solutions, yet the challenge of domain generalization remains largely unaddressed in the literature. To date, the necessity for a new specialized model, which requires significant expertise to construct, persists without a convincing alternative.

3 Methodology

3.1 Gaze Datasets

To assess SAM’s efficacy, we utilized two datasets: the Open Eye Challenge dataset (OpenEDS2019) Garbin et al. (2020), which is widely used to benchmark gaze estimation methods Nair et al. (2020); Chaudhary et al. (2022); Kim et al. (2019); Kothari et al. (2021, 2022); Byrne et al. (2023a), and its successor, the OpenEDS 2020 Challenge dataset (OpenEDS2020) Palmero et al. (2021). OpenEDS2019 Garbin et al. (2020) was collected using a VR head-mounted display (HMD) equipped with two synchronized eye-facing cameras under controlled illumination at a frame rate of 200 Hz. The dataset encompasses eye-region video footage from 152 individual participants, comprising a total of 12,759 images at a resolution of 400×640 pixels, coupled with pixel-level annotation masks for key eye-regions, namely the pupil, iris, and sclera. For a complete description of the data, refer to the original paper Garbin et al. (2020). The OpenEDS 2020 Challenge dataset Palmero et al. (2021) consists of eye-image sequences recorded through a VR HMD mounted with dual eye-facing cameras under controlled lighting conditions at a frame rate of 100 Hz and recorded from 80 participants while performing various gaze-related tasks. It is further separated into two subsets: 1) Gaze Prediction Dataset and 2) Eye Segmentation Dataset. The latter consists of 200 sequences sampled at 5 Hz accompanied by manually annotated segmentation labels for 5% of the dataset, totaling 2605 images at a resolution of 640×400 pixels. A representative image from each dataset is displayed in Fig. 3. Before being fed into SAM’s image encoder, each image is converted to RGB with a pixel intensity range of $[0, 255]$. No further adjustments to the images were performed.

As part of each challenge, the challenge authors conducted baseline experiments to evaluate performance on both datasets. Specifically, they trained an encoder-decoder neural network derived from the SegNet architecture Badrinarayanan et al. (2017) for each dataset. For OpenEDS2019, the model was trained for 200 epochs on the training set provided in the challenge dataset, achieving a mean intersection over union (mIoU) score of 91.4% on the test set consisting of all three features. For OpenEDS2020, the authors trained the model for 150 epochs on the subset of images that had corresponding segmentation masks, reporting a mIoU score of 84.1% across all features.

3.2 Prompting Strategies

We assess SAM’s performance on eye images, utilizing both the automatic “everything” mode and the manual prompting mode, and employing a combination of bounding box and point prompts. SAM’s main strength lies in its capability to

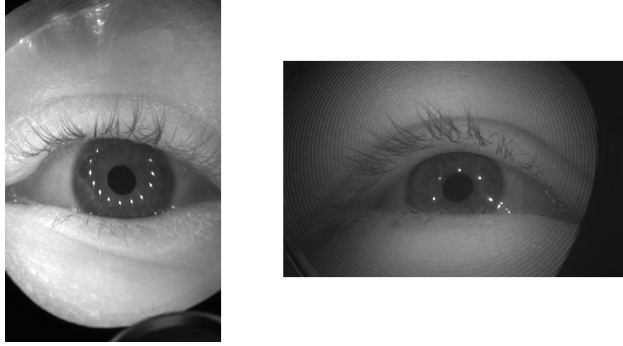


Figure 3: Representative images from OpenEDS2019 Garbin et al. (2020) (left) and OpenEDS2020 Palmero et al. (2021) (right) datasets. Both datasets are captured using a VR head-mounted display equipped with dual synchronous eye-facing cameras. The OpenEDS2019 dataset contains images with a resolution of 400×640 while the images from the OpenEDS2020 dataset have a resolution 640×400 .

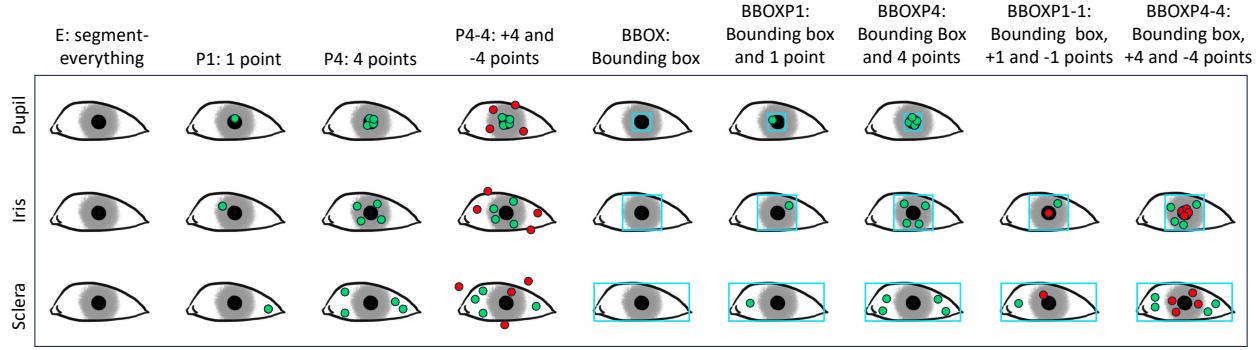


Figure 4: Prompt strategies for segmenting pupil, iris, and sclera. Green points represent foreground point prompts, while red points represent background point prompts. Bounding box prompts are visualized as light blue rectangles surrounding the feature of interest.

incorporate prompts, making it imperative to evaluate the impact of different prompt strategies on model performance. We designed a set of prompting strategies that could be employed by a human annotator using SAM for eye image annotation, as depicted in Fig. 4. Each prompt strategy is described below.

3.2.1 Automated/no prompting

This mode generates all potential segmentations identified by SAM within the image. In the context of data annotation, upon feeding the image to the model, the user receives a series of masks as output. However, not all these segmentations may align with the user’s needs. Consequently, the user may opt to manually choose the masks that best align with the features relevant to them. To simulate this, we adopt the mask-matching mechanism proposed by Huang et al. [2023], which involves identifying masks with the closest Dice scores to the ground truth masks representing the pupil, iris, and sclera. Subsequently, the masks with the highest scores are considered as the model’s predicted features for the given image. We refer to this strategy as E (everything) in our results.

3.2.2 Manual prompting

SAM gives users the flexibility to use diverse prompt strategies to select the feature to segment. Possible strategies include clicking within or outside the region of interest, drawing a loose or tight bounding box around it, or a combination of these approaches. While an exhaustive comparison of all potential prompt strategies is unfeasible, we can categorize these strategies into the following actions: using a point prompt, using multiple point prompts, using a bounding box, and a combination thereof. In this mode, we specifically focus our analysis of SAM’s performance on the following prompt designs, visually depicted in Fig. 4:

1. **Point prompts (P1, P4):** single or multiple (4) points are randomly positioned anywhere on the ground truth mask.
2. **Positive and negative point prompts (P4-4):** taking inspiration from Huang et al. [2023], 4 positive (foreground) points are randomly positioned on the ground truth mask. A bounding box around the ground truth mask is then calculated and doubled in size. 4 negative points are placed outside the ground truth mask within the resulting bounding box.
3. **Bounding Box (BBOX):** a tight bounding box surrounding the ground truth mask.
4. **Bounding Box with point prompts (BBOXP1, BBOXP4):** a tight bounding box surrounding the ground truth mask and a single or multiple (4) point prompts positioned randomly anywhere on the ground truth mask.
5. **Bounding Box with positive and negative point prompts (BBOXP1-1, BBOXP4-4):** To assist SAM in excluding “holes” within the iris and sclera segmentations, we provide it with a tight bounding box and a single or 4 positive point prompts placed randomly on the ground truth mask (the same as BBOXP1 and BBOXP4). We furthermore provide SAM with the same number of negative point prompts placed on the ground truth iris mask (when segmenting the sclera) or on the pupil mask (when segmenting the iris). In this experiment, images where the “holes” are not present (i.e. in cases where the eye is half-covered by the eyelid or in the process of blinking such that the sclera is visible but not the iris, or the iris is visible but not the pupil) are skipped. This strategy furthermore does not apply to pupil segmentation.

Furthermore, we explore the impact on SAM’s performance when introducing variability in the bounding box strategy (BBOX). Taking inspiration from Mattjie et al. [2023], we adjust the bounding box around the ground truth mask, modifying its size and position by 5%, 10%, and 20%. This variation mirrors the potential differences that may arise when different annotators draw bounding boxes over the image.

Across all strategies, images where the targeted feature is absent are excluded. In other words, if SAM’s ability to segment a specific feature (e.g., pupil) is being evaluated, images in which that feature is not present are skipped.

3.3 Evaluation

To evaluate SAM’s segmentation quality, we want to analyze the overlap between its segmentations and the ground truth masks, while also gauging the alignment of the two masks. To measure this, we chose well-established metrics that are commonly used in evaluating image segmentation models:

Dice similarity coefficient (Dice) Milletari et al. (2016): a similarity metric that gauges the overlap between the ground truth mask and the predicted mask. A higher value signifies better model performance. The Dice coefficient is defined as:

$$Dice = \frac{2 \times |A \cap B|}{|A| + |B|} \quad (1)$$

Intersection-over-union (IoU) Zhou et al. (2019): similar to Dice, it measures the overlap between two masks by getting the ratio of the intersection area to the union area of the segments. IoU requires more precision than Dice as it penalizes both under- and over-segmentation more rigorously. Higher values signify a better model:

$$IoU = \frac{|A \cap B|}{|A \cup B|} \quad (2)$$

Hausdorff Distance (HD) Huttenlocher et al. (1993): a boundary-based metric that quantifies the dissimilarity between two shapes by measuring the maximum distance between points on one boundary to the nearest points on the other boundary. This metric can be used to evaluate the degree of alignment between the boundaries of the predicted and ground truth masks. A lower Hausdorff distance indicates better model performance. Given two sets of finite points A and B and with $d(a, b)$ as the distance between points a and b, the Hausdorff Distance is defined as:

$$H(A, B) = \max(h(A, B), h(B, A)) \quad (3)$$

where

$$h(A, B) = \sup_{a \in A} \inf_{b \in B} d(a, b) \quad (4)$$

where sup represents the supremum operator and inf the infimum operator.

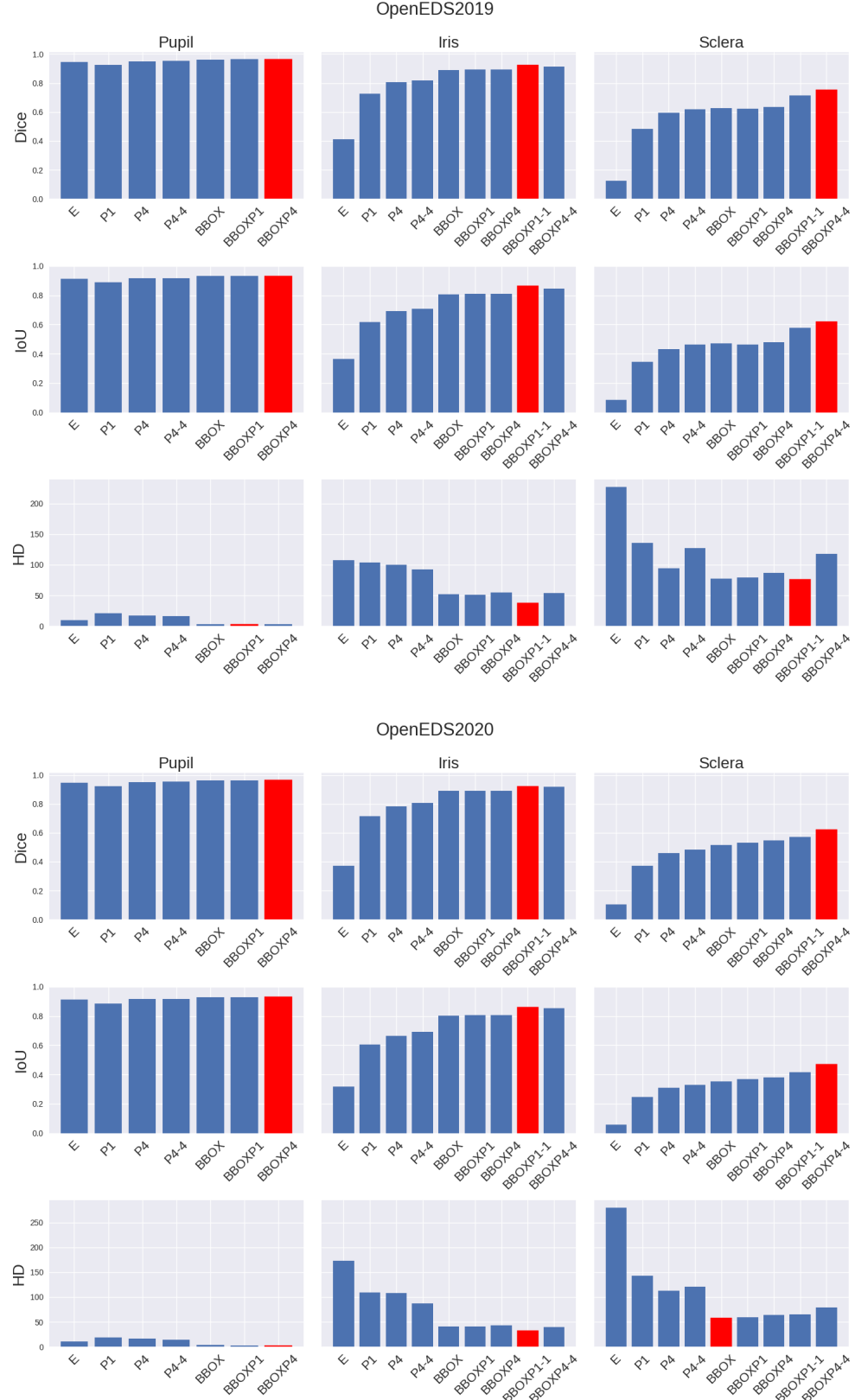


Figure 5: Performance of each strategy on different segmentation tasks (pupil, iris, and sclera segmentation). Each row represents a different metric. On each plot, the best-performing strategy (highest Dice/IoU and lowest HD) is colored red.

OpenEDS-2019										
	Pupil			Iris			Sclera			
Perturbation	5%	10%	20%	5%	10%	20%	5%	10%	20%	
Dice \uparrow	0.9546	0.8423	0.4493	0.8916	0.8775	0.7165	0.6184	0.6021	0.4574	
IoU \uparrow	0.9194	0.7903	0.4086	0.8083	0.7917	0.6261	0.4616	0.4493	0.3330	
HD \downarrow	4.1031	12.1731	37.5265	52.4545	52.9094	63.3940	78.6238	79.8332	92.8560	

OpenEDS-2020										
	Pupil			Iris			Sclera			
Perturbation	5%	10%	20%	5%	10%	20%	5%	10%	20%	
Dice \uparrow	0.9458	0.7849	0.3583	0.8887	0.8763	0.7795	0.5124	0.4701	0.2932	
IoU \uparrow	0.9029	0.7229	0.3244	0.8038	0.7895	0.6830	0.3526	0.3213	0.1967	
HD \downarrow	4.8235	13.9860	37.8557	40.7677	42.4274	54.2700	58.6688	72.2898	144.7311	

Table 1: SAM’s performance on OpenEDS-2019 and -2020 datasets when perturbing the bounding box by 5%, 10%, and 20%

4 Results

Our findings across both datasets demonstrate that SAM’s performance is highly dependent on the type of feature it is segmenting. When segmenting the pupil (refer to Fig. 5, left column), SAM consistently had an IoU score above 88% across both datasets in all strategies, with BBOXP4 yielding the best results with an IoU score of 93.30 % and 93.34% for OpenEDS-2019 and OpenEDS-2020 respectively. When segmenting the iris (Fig. 5, middle column), E performed far more poorly with an IoU score of 36.45% for OpenEDS-2019 and 31.92% for OpenEDS-2020. Meanwhile, the prompting strategies all scored above 60% and BBOXP1-1 was the best-performing strategy with an IoU score of 86.63% and 86.14% for OpenEDS-2019 and OpenEDS-2020 respectively. Lastly, when segmenting the sclera (Fig. 5, right column), SAM performed very poorly compared to when segmenting the pupil and sclera with an IoU score of 8.39% and 5.86% when using the automatic mode. While introducing manual prompts boosted its performance, it reached only an IoU score of 62.19% and 47.06% using BBOXP4-4 for OpenEDS-2019 and OpenEDS-2020 respectively, indicating the need for additional manual guidance.

Comparing across prompting strategies (Fig. 5), E performed reasonably well when segmenting the pupil and even outperformed P1 in both datasets. However, its performance decreased dramatically when segmenting the iris and sclera, in some cases, not overlapping at all with the ground truth mask. This is exemplified by E’s predictions on the sclera in Fig. 6, and 7 which show in both cases that the closest matching segmentation that SAM produces is nowhere near the ground truth mask of the sclera. When introducing point prompts (P1, P4, P4-4), SAM’s performance increased with the number of point prompts used. Using a simple bounding box prompt (BBOX), however, outperformed the use of only point prompts. This is likely because the bounding box more explicitly delineates the area where the feature of interest is located, while point prompts may be ambiguous regarding exactly which object the prompt is referring to. Lastly, a combination of bounding box and point prompts (BBOXP1, BBOXP4, BBOXP1-1, and BBOXP4-4) resulted in the best performance of SAM on both datasets for both the iris and sclera.

Analyzing the impact of perturbed bounding boxes (refer to Table 1), SAM demonstrates a decline in performance with decreasing accuracy of the bounding box placement. However, even when the bounding box is perturbed, SAM still consistently outperforms the majority of the point prompt strategies when segmenting the iris and sclera, particularly with perturbations of 5% and 10%. This observation aligns with the findings of Mattjie et al. [2023], underlining the robustness of the bounding box approach compared to point prompts.

When evaluating SAM’s performance based on the alignment of mask boundaries (refer to Fig. 5, third and last rows), it is evident that strategies incorporating the bounding box prompt consistently yield the best results. However, it is noteworthy that not all strategies deliver the highest degree of alignment (measured by the lowest HD) and the best overlap (measured by the highest IoU and Dice scores) simultaneously. This is particularly evident when examining performance on the sclera. While BBOXP4-4 showed the best overlap for both datasets, it did not show the best alignment. Meanwhile, the BBOXP1-1 strategy showed the best alignment for OpenEDS2019 and BBOX performed best on OpenEDS2020 while these showed up to almost 30% worse overlap scores. This indicates that, although incorporating point prompts with the bounding box prompt may help SAM to capture the general shape of the sclera, it might actually hurt its ability to accurately delineate its exact boundaries. Although less clear, the same trend is seen in

the iris data, where adding a single prompt point to the bounding box lead to better alignment than adding four prompt points.

Choosing the best-performing strategy for the pupil (BBOXP4), iris (BBOXP1-1), and sclera (BBOXP4-4), we calculated the mIoU for each dataset. The results indicated a mIoU of 85.70% and 83.90% on the OpenEDS-2019 and OpenEDS-2020 datasets, respectively. These values fell short of the previously established baselines of 91.4% Garbin et al. (2020) and 84.1% Palmero et al. (2021). This is likely attributed to SAM’s limitations in accurately segmenting the sclera as previously observed. Indeed, upon excluding the results related to sclera, the mIoU improved significantly to 91.38% for OpenEDS2019 and 91.02% for OpenEDS2020. However, these scores still lag behind the top-performing results from the accompanying leaderboards^{2,3}, which achieved a mIoU score of 95.28% for OpenEDS2019 and 95.17% for OpenEDS2020.

5 Discussion

Evaluating the capability of the Segment Anything Model (SAM) in delineating critical eye features for eye tracking, our study reveals that SAM effectively performs zero-shot segmentation on the pupil, achieving an impressive IoU (Intersection over Union) of 93.34%. With the assistance of bounding box and point prompts, it also successfully segments the iris, reaching an IoU of 86.63%. Nevertheless, SAM encounters difficulties with the sclera, achieving a best IoU of only 62.19%, and this limitation persists regardless of the type of prompt used, even though prompts do enhance the performance over its automatic mode. These findings are consistent with previous investigations mainly from the medical imaging sector Mazurowski et al. (2023); Huang et al. (2023).

The fundamental question for those in the eye-tracking field may boil down to “Is SAM suitable for segmenting eye images?” The answer hinges on the specific feature in question. For example, SAM exhibits strong capabilities in pupil segmentation which can be used in pupil detection pipelines, a crucial element in numerous gaze-tracking frameworks Kim et al. (2019), and the primary subject of various studies Fuhl et al. (2016a); Santini et al. (2018); Fuhl et al. (2015). The effectiveness of SAM for segmenting the iris is comparatively lower, compared to the pupil. We attribute this reduction in performance to the iris having a lower contrast and relatively blurred edge with the sclera, conditions that have previously been observed to pose problems for SAM Mattjie et al. (2023); Huang et al. (2023). Moreover, our results reveal that SAM struggles to recognize the sclera as a distinct object and requires extensive guidance from an annotator through the use of manual prompts. We speculate that shadows from the eyelids and non-uniform illumination contribute to large variations in scleral luminance in the images. This, combined with the blurry edge between the iris and the sclera, likely poses a significant challenge for SAM.

6 Limitations and Future Work

Our study presents several limitations. First, our study assessed only the zero-shot capabilities of SAM within a Virtual Reality (VR) environment. Future research should extend the evaluation of SAM’s performance to eye images acquired from wearable as well as high-resolution laboratory eye trackers. High-resolution eye tracking may demand greater precision and the segmentation of different features Byrne et al. (2023a) for which the segmentation techniques utilized in our study may not be effective. The complexity of “gaze-in-the-wild” contexts, characterized by considerable variability in eye appearance and challenges with low image quality, may present a more arduous challenge than VR environments investigated in this paper Kothari et al. (2020); Fuhl et al. (2016b, 2022). Second, there is potential for uncovering more effective prompting strategies that could further enhance the model’s performance in segmenting eye regions. Finally, our study did not address the segmentation of corneal reflections, despite their presence in the images (as demonstrated in Chugh et al. (2021); Maquiling et al. (2023); Byrne et al. (2023a)) because they were not annotated in the dataset. Future work should consider including these reflections, as the detection and matching of these features can be integral to comprehensive eye-tracking analyses and P-CR pipelines Chugh et al. (2021).

This research opens the door to a variety of future research avenues. One promising direction is the fine-tuning of SAM on a small amount of eye images, to investigate if this fine-tuning step improves the results compared to the standard model. Second, developing a foundation model trained on a comprehensive dataset, such as TEyeD Fuhl et al. (2021), could become a pivotal asset for the eye-tracking community. However, this endeavor would necessitate computational resources beyond those typically accessible to a standard laboratory. Another intriguing potential research path involves integrating text prompting into the model to further simplify the annotation process for users without technical expertise.

²<https://eval.ai/web/challenges/challenge-page/353/leaderboard/1002>

³<https://eval.ai/web/challenges/challenge-page/603/leaderboard/1680>

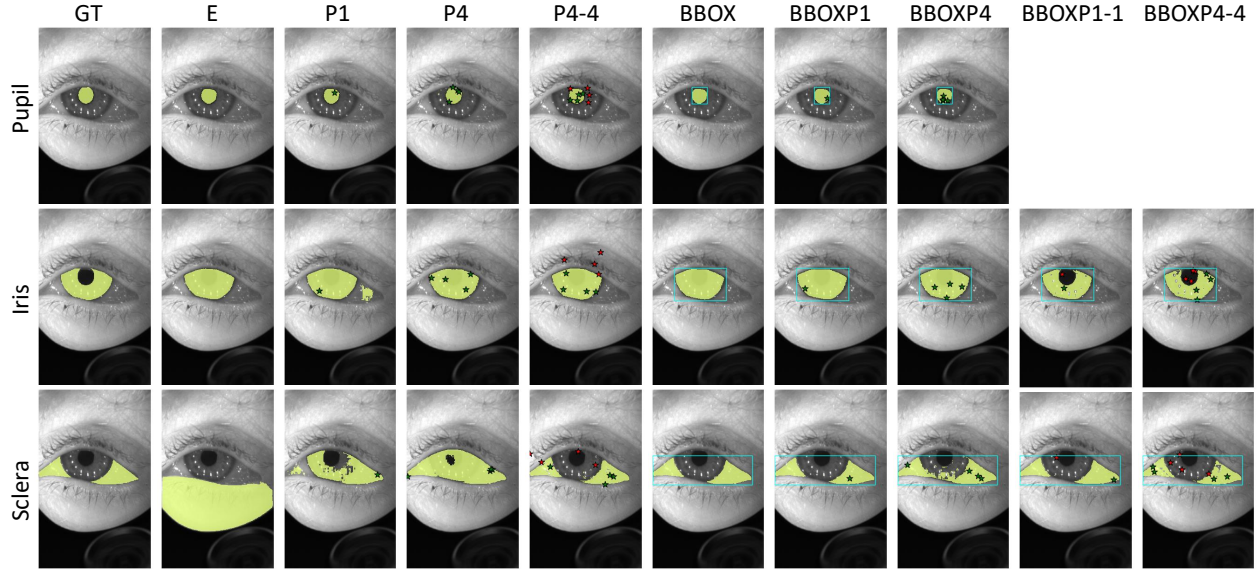


Figure 6: Visualization of SAM’s performance on an image from OpenEDS2019 Garbin et al. (2020). The leftmost column shows the ground truth masks for pupil (top row), iris (middle row), and sclera (bottom row) overlaid on the input image. The remaining columns show SAM’s segmentations using different strategies.

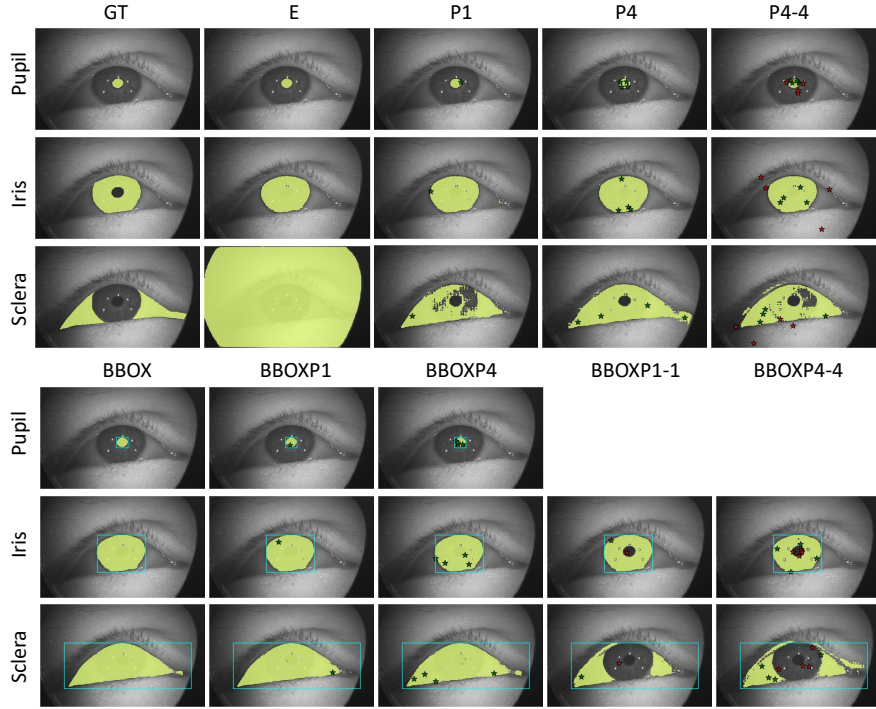


Figure 7: Visualization of SAM’s performance on an image from OpenEDS2020 Palmero et al. (2021)

7 Conclusion

This study explored the applicability of the Segment Anything Model (SAM) for segmenting eye images, the first study into a foundation model’s performance in this specific task to our knowledge. SAM showed promising zero-shot capabilities, particularly in pupil segmentation. While we recommend a cautious approach to using SAM for eye image segmentation in its current state, this technology may represent a paradigm shift away from specialized supervised learning models towards foundational models. However, what the eye-tracking community may need for this technology

to be fully realized is a bespoke foundation model trained on eye images, akin to how MedSAM Ma et al. (2023) is tailored for medical images or RETFound Zhou et al. (2023a) for retinal imaging. Regardless, foundation models offer an exciting new direction for the field. They could reduce the technical barriers associated with developing specialized models, mitigate the acute shortage of annotated datasets required for training deep learning systems, and achieve domain generalization—critical challenges in gaze estimation. This shift has the potential to democratize eye-tracking technologies, particularly as VR systems become increasingly mainstream, enabling new market entrants to compete with established companies by leveraging the scalable utility of foundation models.

References

Anwai Archit, Sushmita Nair, Nabeel Khalid, Paul Hilt, Vikas Rajashekhar, Marei Freitag, Sagnik Gupta, Andreas Dengel, Sheraz Ahmed, and Constantin Pape. 2023. Segment Anything for Microscopy. *bioRxiv* (2023), 2023–08.

Vijay Badrinarayanan, Alex Kendall, and Roberto Cipolla. 2017. Segnet: A deep convolutional encoder-decoder architecture for image segmentation. *IEEE transactions on pattern analysis and machine intelligence* 39, 12 (2017), 2481–2495.

Rishi Bommasani, Drew A. Hudson, Ehsan Adeli, Russ Altman, Simran Arora, Sydney von Arx, Michael S. Bernstein, Jeannette Bohg, Antoine Bosselut, Emma Brunskill, Erik Brynjolfsson, Shyamal Buch, Dallas Card, Rodrigo Castellon, Niladri Chatterji, Annie Chen, Kathleen Creel, Jared Quincy Davis, Dora Demszky, Chris Donahue, Moussa Doumbouya, Esin Durmus, Stefano Ermon, John Etchemendy, Kawin Ethayarajh, Li Fei-Fei, Chelsea Finn, Trevor Gale, Lauren Gillespie, Karan Goel, Noah Goodman, Shelby Grossman, Neel Guha, Tatsunori Hashimoto, Peter Henderson, John Hewitt, Daniel E. Ho, Jenny Hong, Kyle Hsu, Jing Huang, Thomas Icard, Saahil Jain, Dan Jurafsky, Pratyusha Kalluri, Siddharth Karamcheti, Geoff Keeling, Fereshte Khani, Omar Khattab, Pang Wei Koh, Mark Krass, Ranjay Krishna, Rohith Kuditipudi, Ananya Kumar, Faisal Ladhak, Mina Lee, Tony Lee, Jure Leskovec, Isabelle Levent, Xiang Lisa Li, Xuechen Li, Tengyu Ma, Ali Malik, Christopher D. Manning, Suvir Mirchandani, Eric Mitchell, Zanele Munyikwa, Suraj Nair, Avanika Narayan, Deepak Narayanan, Ben Newman, Allen Nie, Juan Carlos Niebles, Hamed Nilforoshan, Julian Nyarko, Giray Ogut, Laurel Orr, Isabel Papadimitriou, Joon Sung Park, Chris Piech, Eva Portelance, Christopher Potts, Aditi Raghunathan, Rob Reich, Hongyu Ren, Frieda Rong, Yusuf Roohani, Camilo Ruiz, Jack Ryan, Christopher Ré, Dorsa Sadigh, Shiori Sagawa, Keshav Santhanam, Andy Shih, Krishnan Srinivasan, Alex Tamkin, Rohan Taori, Armin W. Thomas, Florian Tramèr, Rose E. Wang, William Wang, Bohan Wu, Jiajun Wu, Yuhuai Wu, Sang Michael Xie, Michihiro Yasunaga, Jiaxuan You, Matei Zaharia, Michael Zhang, Tianyi Zhang, Xikun Zhang, Yuhui Zhang, Lucia Zheng, Kaitlyn Zhou, and Percy Liang. 2022. On the Opportunities and Risks of Foundation Models. *arXiv:2108.07258 [cs.LG]*

Tom B. Brown, Benjamin Mann, Nick Ryder, Melanie Subbiah, Jared Kaplan, Prafulla Dhariwal, Arvind Neelakantan, Pranav Shyam, Girish Sastry, Amanda Askell, Sandhini Agarwal, Ariel Herbert-Voss, Gretchen Krueger, Tom Henighan, Rewon Child, Aditya Ramesh, Daniel M. Ziegler, Jeffrey Wu, Clemens Winter, Christopher Hesse, Mark Chen, Eric Sigler, Mateusz Litwin, Scott Gray, Benjamin Chess, Jack Clark, Christopher Berner, Sam McCandlish, Alec Radford, Ilya Sutskever, and Dario Amodei. 2020. Language Models are Few-Shot Learners. *arXiv:2005.14165 [cs.CL]*

Sean Anthony Byrne, Virmarie Maquiling, Marcus Nyström, Enkelejda Kasneci, and Diederick C Niehorster. 2023a. LEyes: A Lightweight Framework for Deep Learning-Based Eye Tracking using Synthetic Eye Images. *arXiv preprint arXiv:2309.06129* (2023).

Sean Anthony Byrne, Marcus Nyström, Virmarie Maquiling, Enkelejda Kasneci, and Diederick C Niehorster. 2023b. Precise localization of corneal reflections in eye images using deep learning trained on synthetic data. *arXiv preprint arXiv:2304.05673* (2023).

Aayush K Chaudhary, Nitinraj Nair, Reynold J Bailey, Jeff B Pelz, Sachin S Talathi, and Gabriel J Diaz. 2022. Temporal RIT-Eyes: From real infrared eye-images to synthetic sequences of gaze behavior. *IEEE Transactions on Visualization and Computer Graphics* 28, 11 (2022), 3948–3958.

Soumil Chugh, Braiden Brousseau, Jonathan Rose, and Moshe Eizenman. 2021. Detection and correspondence matching of corneal reflections for eye tracking using deep learning. In *2020 25th International Conference on Pattern Recognition (ICPR)*. IEEE, 2210–2217.

Jacob Devlin, Ming-Wei Chang, Kenton Lee, and Kristina Toutanova. 2018. Bert: Pre-training of deep bidirectional transformers for language understanding. *arXiv preprint arXiv:1810.04805* (2018).

Alexey Dosovitskiy, Lucas Beyer, Alexander Kolesnikov, Dirk Weissenborn, Xiaohua Zhai, Thomas Unterthiner, Mostafa Dehghani, Matthias Minderer, Georg Heigold, Sylvain Gelly, et al. 2010. An image is worth 16x16 words: Transformers for image recognition at scale. *arXiv* 2020. *arXiv preprint arXiv:2010.11929* (2010).

Matt J Dunn, Robert G Alexander, Onyekachukwu M Amiebenomo, Gemma Arblaster, Denize Atan, Jonathan T Erichsen, Ulrich Ettinger, Mario E Giardini, Iain D Gilchrist, Ruth Hamilton, et al. 2023. Minimal reporting guideline for research involving eye tracking (2023 edition). *Behavior research methods* (2023), 1–7.

Wolfgang Fuhl, Gjergji Kasneci, and Enkelejda Kasneci. 2021. TEyeD: Over 20 Million Real-World Eye Images with Pupil, Eyelid, and Iris 2D and 3D Segmentations, 2D and 3D Landmarks, 3D Eyeball, Gaze Vector, and Eye Movement Types. In *2021 IEEE International Symposium on Mixed and Augmented Reality (ISMAR)*. IEEE. <https://doi.org/10.1109/ismar52148.2021.00053>

Wolfgang Fuhl, Thomas Kübler, Katrin Sippel, Wolfgang Rosenstiel, and Enkelejda Kasneci. 2015. Excuse: Robust pupil detection in real-world scenarios. In *Computer Analysis of Images and Patterns: 16th International Conference, CAIP 2015, Valletta, Malta, September 2-4, 2015 Proceedings, Part I* 16. Springer, 39–51.

Wolfgang Fuhl, Thiago Santini, Gjergji Kasneci, and Enkelejda Kasneci. 2016a. Pupilnet: Convolutional neural networks for robust pupil detection. *arXiv preprint arXiv:1601.04902* (2016).

Wolfgang Fuhl, Marc Tonsen, Andreas Bulling, and Enkelejda Kasneci. 2016b. Pupil detection for head-mounted eye tracking in the wild: an evaluation of the state of the art. *Machine Vision and Applications* 27 (2016), 1275–1288.

Wolfgang Fuhl, Daniel Weber, and Shahram Eivazi. 2022. Pistol: Pupil invisible supportive tool to extract pupil, iris, eye opening, eye movements, pupil and iris gaze vector, and 2d as well as 3d gaze. *arXiv preprint arXiv:2201.06799* (2022).

Stephan Joachim Garbin, Oleg Komogortsev, Robert Cavin, Gregory Hughes, Yiru Shen, Immo Schuetz, and Sachin S Talathi. 2020. Dataset for eye tracking on a virtual reality platform. In *ACM Symposium on Eye Tracking Research and Applications*. 1–10.

Kaiming He, Xinlei Chen, Saining Xie, Yanghao Li, Piotr Dollár, and Ross Girshick. 2022. Masked autoencoders are scalable vision learners. In *Proceedings of the IEEE/CVF conference on computer vision and pattern recognition*. 16000–16009.

Kenneth Holmqvist, Marcus Nyström, Richard Andersson, Richard Dewhurst, Halszka Jarodzka, and Joost Van de Weijer. 2011. *Eye tracking: A comprehensive guide to methods and measures*. OUP Oxford.

Yuhao Huang, Xin Yang, Lian Liu, Han Zhou, Ao Chang, Xinrui Zhou, Rusi Chen, Junxuan Yu, Jiongquan Chen, Chaoyu Chen, Haozhe Chi, Xindi Hu, Deng-Ping Fan, Fajin Dong, and Dong Ni. 2023. Segment Anything Model for Medical Images? *arXiv:2304.14660* [eess.IV]

Daniel P Huttenlocher, Gregory A. Klanderman, and William J Rucklidge. 1993. Comparing images using the Hausdorff distance. *IEEE Transactions on pattern analysis and machine intelligence* 15, 9 (1993), 850–863.

Yongcheng Jing, Xinchao Wang, and Dacheng Tao. 2023. Segment Anything in Non-Euclidean Domains: Challenges and Opportunities. *arXiv:2304.11595* [cs.CV]

Joohwan Kim, Michael Stengel, Alexander Majercik, Shalini De Mello, David Dunn, Samuli Laine, Morgan McGuire, and David Luebke. 2019. Nvgaze: An anatomically-informed dataset for low-latency, near-eye gaze estimation. In *Proceedings of the 2019 CHI conference on human factors in computing systems*. 1–12.

Alexander Kirillov, Eric Mintun, Nikhila Ravi, Hanzi Mao, Chloe Rolland, Laura Gustafson, Tete Xiao, Spencer Whitehead, Alexander C. Berg, Wan-Yen Lo, Piotr Dollár, and Ross Girshick. 2023. Segment Anything. *arXiv:2304.02643* [cs.CV]

Rakshit Kothari, Zhizhuo Yang, Christopher Kanan, Reynold Bailey, Jeff B Pelz, and Gabriel J Diaz. 2020. Gaze-in-wild: A dataset for studying eye and head coordination in everyday activities. *Scientific reports* 10, 1 (2020), 2539.

Rakshit S Kothari, Reynold J Bailey, Christopher Kanan, Jeff B Pelz, and Gabriel J Diaz. 2022. EllSeg-Gen, towards Domain Generalization for head-mounted eyetracking. *Proceedings of the ACM on Human-Computer Interaction* 6, ETRA (2022), 1–17.

Rakshit S Kothari, Aayush K Chaudhary, Reynold J Bailey, Jeff B Pelz, and Gabriel J Diaz. 2021. Ellseg: An ellipse segmentation framework for robust gaze tracking. *IEEE Transactions on Visualization and Computer Graphics* 27, 5 (2021), 2757–2767.

Jun Ma, Yuting He, Feifei Li, Lin Han, Chenyu You, and Bo Wang. 2023. Segment Anything in Medical Images. *arXiv:2304.12306* [eess.IV]

Virmarie Maquiling, Sean Anthony Byrne, Marcus Nyström, Enkelejda Kasneci, and Diederick C Niehorster. 2023. V-ir-Net: A Novel Neural Network for Pupil and Corneal Reflection Detection trained on Simulated Light Distributions. In *Proceedings of the 25th International Conference on Mobile Human-Computer Interaction*. 1–7.

Christian Mattjie, Luis Vinicius de Moura, Rafaela Cappelari Ravazio, Lucas Silveira Kupssinskü, Otávio Parraga, Marcelo Mussi Delucis, and Rodrigo Coelho Barros. 2023. Zero-shot performance of the Segment Anything Model (SAM) in 2D medical imaging: A comprehensive evaluation and practical guidelines. *arXiv:2305.00109 [cs.CV]*

Maciej A Mazurowski, Haoyu Dong, Hanxue Gu, Jichen Yang, Nicholas Konz, and Yixin Zhang. 2023. Segment anything model for medical image analysis: an experimental study. *Medical Image Analysis* 89 (2023), 102918.

Fausto Milletari, Nassir Navab, and Seyed-Ahmad Ahmadi. 2016. V-net: Fully convolutional neural networks for volumetric medical image segmentation. In *2016 fourth international conference on 3D vision (3DV)*. Ieee, 565–571.

Nitinraj Nair, Rakshit Kothari, Aayush K Chaudhary, Zhizhuo Yang, Gabriel J Diaz, Jeff B Pelz, and Reynold J Bailey. 2020. RIT-Eyes: Rendering of near-eye images for eye-tracking applications. In *ACM Symposium on Applied Perception 2020*. 1–9.

Cristina Palmero, Abhishek Sharma, Karsten Behrendt, Kapil Krishnakumar, Oleg V Komogortsev, and Sachin S Talathi. 2021. Openeds2020 challenge on gaze tracking for vr: Dataset and results. *Sensors* 21, 14 (2021), 4769.

Alec Radford, Jong Wook Kim, Chris Hallacy, Aditya Ramesh, Gabriel Goh, Sandhini Agarwal, Girish Sastry, Amanda Askell, Pamela Mishkin, Jack Clark, Gretchen Krueger, and Ilya Sutskever. 2021. Learning Transferable Visual Models From Natural Language Supervision. *arXiv:2103.00020 [cs.CV]*

Bernardino Romera-Paredes and Philip Torr. 2015. An embarrassingly simple approach to zero-shot learning. In *Proceedings of the 32nd International Conference on Machine Learning (Proceedings of Machine Learning Research, Vol. 37)*, Francis Bach and David Blei (Eds.). PMLR, Lille, France, 2152–2161. <https://proceedings.mlr.press/v37/romera-paredes15.html>

Thiago Santini, Wolfgang Fuhl, and Enkelejda Kasneci. 2018. PuRe: Robust pupil detection for real-time pervasive eye tracking. *Computer Vision and Image Understanding* 170 (2018), 40–50.

Qiuhong Shen, Xingyi Yang, and Xinchao Wang. 2023. Anything-3d: Towards single-view anything reconstruction in the wild. *arXiv preprint arXiv:2304.10261* (2023).

Bin Wang, Armstrong Aboah, Zheyuan Zhang, and Ulas Bagci. 2023a. Gazesam: What you see is what you segment. *arXiv preprint arXiv:2304.13844* (2023).

Di Wang, Jing Zhang, Bo Du, Dacheng Tao, and Liangpei Zhang. 2023b. Scaling-up remote sensing segmentation dataset with segment anything model. *arXiv preprint arXiv:2305.02034* (2023).

Jinyu Yang, Mingqi Gao, Zhe Li, Shang Gao, Fangjing Wang, and Feng Zheng. 2023. Track Anything: Segment Anything Meets Videos. *arXiv:2304.11968 [cs.CV]*

Ce Zhou, Qian Li, Chen Li, Jun Yu, Yixin Liu, Guangjing Wang, Kai Zhang, Cheng Ji, Qiben Yan, Lifang He, et al. 2023b. A comprehensive survey on pretrained foundation models: A history from bert to chatgpt. *arXiv preprint arXiv:2302.09419* (2023).

Dingfu Zhou, Jin Fang, Xibin Song, Chenye Guan, Junbo Yin, Yuchao Dai, and Ruigang Yang. 2019. Iou loss for 2d/3d object detection. In *2019 international conference on 3D vision (3DV)*. IEEE, 85–94.

Kaiyang Zhou, Ziwei Liu, Yu Qiao, Tao Xiang, and Chen Change Loy. 2022. Domain generalization: A survey. *IEEE Transactions on Pattern Analysis and Machine Intelligence* (2022).

Yukun Zhou, Mark A Chia, Siegfried K Wagner, Murat S Ayhan, Dominic J Williamson, Robbert R Struyven, Timing Liu, Moucheng Xu, Mateo G Lozano, Peter Woodward-Court, et al. 2023a. A foundation model for generalizable disease detection from retinal images. *Nature* (2023), 1–8.